Article

Electron Tunneling in Biology: When Does it Matter?

Setare M. Sarhangi[1] and Dmitry V. Matyushov [2,*]

[1] Department of Physics, Arizona State University, PO Box 871504, Tempe, Arizona 85287-1504, USA; smostaj1@asu.edu
[2] School of Molecular Sciences and Department of Physics, Arizona State University, PO Box 871504, Tempe, Arizona 85287-1504, USA; dmitrym@asu.edu
* Correspondence: dmitrym@asu.edu.

Abstract: Electron can tunnel between cofactor molecules positioned along biological electron transport chains up to the distance of $\simeq$ 20 Å on the millisecond time scale of enzymatic turnover. This tunneling range mostly determines the design of biological energy chains facilitating cross-membrane transport of electrons. Tunneling distance and cofactors' redox potentials become main physical parameters of this design. The protein identity, flexibility, or dynamics are missing from this picture assigning universal charge-transport properties to all proteins. This paradigm is challenged by dynamical models of electron transfer showing that the hopping rate is constant within the crossover distance $R^* \simeq 12$ Å, followed with an exponential tunneling falloff at longer distances. In this view, energy chains for electron transport are best designed by placing redox cofactors near the crossover distance R^*. Protein flexibility and dynamics affect the magnitude of the maximum hopping rate within the crossover radius. Protein charge transport is not driven by universal parameters anymore and protein identity matters.

Keywords: Protein electron transfer; tunneling; protein dynamics; electrowetting; Stokes-shift dynamics

1. Introduction

Experimental studies of tunneling in biology were initiated by 1966 paper by DeVault and Chance [1]. They reported the kinetics of oxidation of cytochrome proteins by the photoexcited reaction center of the photosynthetic bacterium *Chromatium*. The half-time of the reaction was found to increase from $\simeq 2$ μs at room temperature to $\simeq$ 2.3 ms at 100 K and stayed nearly constant down to 35 K (Figure 1). Even though the fast component of the reaction showed activated Arrhenius kinetics in the entire range of temperatures, the slow decay was found to be "a very nearly if not actually temperature independent" [1]. Tunneling was proposed to explain observations and that set in motion an extensive research program to study tunneling and, more generally, quantum effects in biology [2].

Tunneling is presently an accepted view for transport of two subatomic particles responsible for all energy of life: the electron and the proton [2]. The cross-membrane separation of electrons and protons is the basis of Mitchell's chemiosmotic hypothesis [3,4]: the cross-membrane protonmotive force provides free energy for the synthesis of ATPs required for cellular function. The question that has hunted several generations of scientists is whether transport of charges occurs as a coherent process, through conduction bands [5–7], or through decoherent tunneling hops between sites of charge localization. Despite a number of suggestions of coherent transport through biopolymers [8,9], the prevailing view is that intraprotein charge transport occurs through decoherent hops between redox cofactors intercalated in the protein fold [10,11]. Proteins can also polymerize in nanowires to deliver electrons over micrometer distances in the process called extracellular electron transfer [12,13]. However, in that case as well the prevailing conductivity mechanism is thought to be incoherent hops between sites of electron localization [14–16].

Preprints (www.preprints.org) | NOT PEER-REVIEWED | Posted: 14 November 2022 doi:10.20944/preprints202211.0232.v1

Tunneling of electrons between localized states follows Gamow's view [17] of under-barrier transition probability between two unperturbed stationary eigenstates at two opposite sides of the tunneling barrier. If the energies of quantum states involved in tunneling are equal, the probability of penetrating the barrier scales exponentially $\propto \exp[-\gamma R]$ with the barrier width R. This exponential falloff with the distance between the centers of electron localization (the donor and acceptor) is retained in so-called electronic coupling promoting electronic radiationless transitions (without a photon involved [18])

$$V(R) \propto \exp\left[-\tfrac{1}{2}\gamma R\right], \tag{1}$$

The electronic coupling is the perturbation of the electronic Hamiltonian that brings about electronic transitions between electronic states spatially localized at the donor and acceptor. It defines the rate constant for electronic transitions according to Fermi's golden rule equation [19]

$$k_{\mathrm{NA}} = \frac{2\pi}{\hbar}\left\langle V(R)^2\delta(X)\right\rangle. \tag{2}$$

The rate constant k_{NA} describes the single-exponential decay of the population of the donor state when transitions are initiated. This is typically done by photoexcitation [20], as was realized by photoexciting the reaction center's primary pair in DeVault and Chance experiments [1].

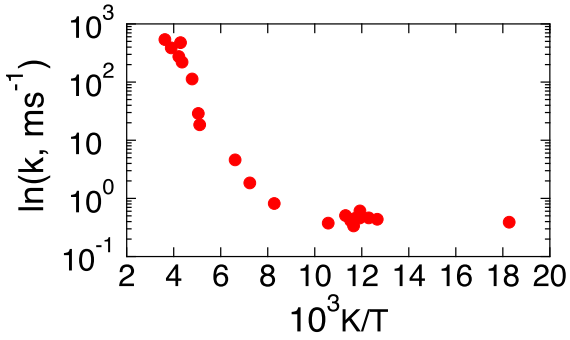

Figure 1. Rate constant for cytochrome oxidation by photoexcited reaction center of the photosynthetic bacterium *Chromatium* [1]. The activation barrier is nearly zero at $T < 100$ K as explained by prevalence of the tunneling mechanism. Reproduced with permission from Ref [1].

The reaction coordinate X in Eq. (2) was introduced by Lax [18] and later by Warshel [21] as the natural coordinate monitoring the progress of a radiationless transition. Given that resonance of the initial and final energies is required for tunneling, it is defined as the difference (energy gap) between the final, $E_2(\mathbf{q})$, and initial, $E_1(\mathbf{q})$, energies

$$X(\mathbf{q}) = E_2(\mathbf{q}) - E_1(\mathbf{q}). \tag{3}$$

The delta-function $\delta(X)$ in Eq. (2) imposes the condition $X(\mathbf{q}) = 0$ of tunneling resonance when the energies of initial and final states become equal. Finally, reactions following the golden rule recipe are labeled as "non-adiabatic" reactions, as specified by the corresponding subscript in Eq. (2).

The energy states $E_i(\mathbf{q})$, $i = 1, 2$ depend on the manifold of nuclear coordinates $\mathbf{q}$ affecting the electronic states. The average $\langle \dots \rangle$ in Eq. (2) is taken over the statistical configurations of those nuclear coordinates. The donor-acceptor distance R can fluctuate as the result of thermal motions and generally should be included in the statistical average [22].

If the donor-acceptor complex is sufficiently rigid, one can separate the electronic coupling at the equilibrium donor acceptor distance R_e from fluctuations of the coupling due

Preprints (www.preprints.org) | NOT PEER-REVIEWED | Posted: 14 November 2022 doi:10.20944/preprints202211.0232.v1

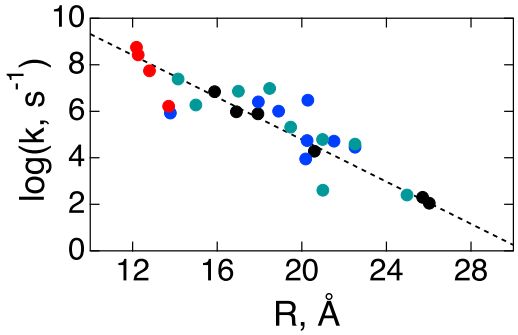

Figure 2. Rate constants of activatioless electron transfer vs the donor-acceptot distance for Ru-modified proteins: azurin (black), cytochrome c (blue), cytochrome c-b562 (cyan), and high-potential iron protein (red). The dashed black line is drawn through the azurin data with the exponential decay constant of 1.04 Å^{-1}. The experimental results (points) are reproduced with permission from Ref. [24].

to distance changes $\delta R = R - R_e$. One therefore finds that the rate constant is proportional to V_e^2 and exponentially decays with the equilibrium distance

$$k_{\rm NA} \propto V_e^2 \propto e^{-\gamma R_e}. \tag{4}$$

Significant body of experimental work went into studies of the distance decay of the electron-transfer rate constant. Specifically, Winkler and Gray introduced the technique of attaching a photo-excitable Ru^{II} complex to the surface of a redox-active protein. By varying the attachment site, an impressive range of distances was sampled [11,23,24] (Figure 2). These studies have resulted in an average value of the tunneling decay parameter assigned to protein media and equal to $\gamma \simeq 1.1 - 1.2$ Å^{-1}. A similar value, $\gamma \simeq 1.4$ Å^{-1}, was extracted from studies of kinetics of photosynthetic reactions [25,26] (Figure 3).

The available data point out that the combination of electronic coupling and the activation barrier $\Delta F^\dagger$ are sufficient to describe protein electron transfer [26]. The rate constant is obtained by taking the statistical average over the delta-function in Eq. (2). This goal can be achieved within the framework of Marcus theory [27] considering Gaussian fluctuations of the medium bringing the initial and final energies into resonance. Th result is given by the following expression

$$k_{\rm NA} \propto V_e^2 e^{-\beta \Delta F^\dagger}, \tag{5}$$

where $\beta = (k_{\rm B}T)^{-1}$ is the inverse temperature and the activation barrier in Marcus theory is specified by two parameters, the reaction free energy ΔF_0 and the reorganization energy λ

$$\Delta F^\dagger = \frac{(\lambda + \Delta F_0)^2}{4\lambda}. \tag{6}$$

A "universal" value of the reorganization energy $\lambda \simeq 0.8$ eV was suggested to apply to protein electron transfer [25].

The combination of equations (5) and (6) offers a universal picture of electron transfer in protein media. Both the decal parameter γ and the reorganization energy λ are viewed as parameters generic to protein media. The only parameters left to tune the rate are the donor-acceptor distance and the reaction free energy. This picture also suggests that the closest packing of cofactors as allowed by steric constraints of electron-transport chains provides the best strategy to optimize their performance. The placement of cofactors in such chains is limited by the universal donor-acceptor distance $R_D \simeq 12 - 15$ Å (Dutton radius [25]) for reactions with zero reaction free energy, which can be extended to $\simeq 21$ Å for activationless transitions [24] ($-\Delta F_0 = \lambda$ in Eq. (6)).

Preprints (www.preprints.org) | NOT PEER-REVIEWED | Posted: 14 November 2022 doi:10.20944/preprints202211.0232.v1

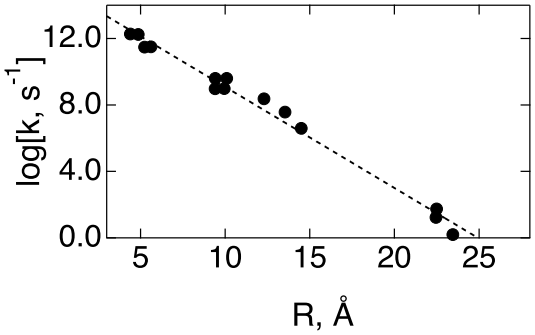

Figure 3. Rate constants of electron transfer in photosynthetic reaction centers vs the edge-to-edge distance between the redox cofactors (points). The rate constants are recalculated to the values of zero activation barrier. The dashed line is the linear fits through the point with the slope $\gamma = 1.4$ Å^{-1}. The plot is adopted with permission from Ref. [10].

The universal, based on golden rule (Eq. (2)) view of electron transfer comes in stark contrast to a number of early and modern ideas advocated to expalin the catalytic effect of the protein medium on enzymatic reactions. An early explanation of the catalytic effect is due to Pauling [28], who suggested that enzymes preferentially stabilize the activated state of the reaction thus reducing the barrier. This notion is clearly inconsistent with the theory of nonadiabatic electron transfer operating with equilibrium free energies (λ and ΔF_0) and not involving any notion of the transition-state configuration and its energy. A more recent suggestion involves non-statistical, dynamical aspects of protein flexibility [29] as a potential reason for the catalytic effect [30–32]. It is nevertheless obvious that none of these concepts have entered the present formulation of the theory of protein electron transfer. The present-day universal theory does not involve individual properties of a specific protein, such as dynamics, elasticity, conformational flexibility, etc. The formalism discussed here aims to change this view.

We offer a formalism that incorporates protein elasticity into the rate of electron transfer in the form of elastic modulation of the tunneling probability. The resulting formulation predicts that most intraprotein electron-transfer reactions are controlled by the medium dynamics and not by tunneling probability. Tunneling becomes important only at distances exceeding the crossover distance R^* at which the dynamical control of the rate constant is switched to the tunneling control. Therefore, no reaction speedup can be achieved by placing redox cofactors at distances closer than the crossover distance and optimum rate of electron transport is achieved when cofactors are placed at separations close to R^*.

The demand to develop a framework alternative to the theory of nonadiabatic electron transfer (Eqs. (5) and (6)) came from a somewhat unexpected direction. Advances in electrochemistry of redox species attached to monolayers self-assembled at the metal electrode [33] have led to the development of thin-film electrochemistry of redox-active proteins [34–37]. This technique provides the dependence of the electrochemical rate constant on the thickness of the monolayer, i.e., on the tunneling distance [38–41]. While the value $\gamma \simeq 1$ Å^{-1} from solution studies (Figures 2 and 3) was confirmed by electrochemical measurements, unexpected results have also emerged.

Preprints (www.preprints.org) | NOT PEER-REVIEWED | Posted: 14 November 2022 doi:10.20944/preprints202211.0232.v1

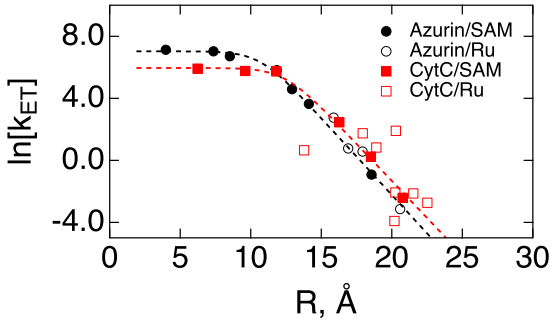

Figure 4. Apparent rate constants of electron transfer between a metal electrode and different proteins immobilized on SAMs of varying thickness: azurin (black) and cytochrome c on CO_2^--terminated SAMs (CytC, red). The dashed lines are fits to Eq. (8) assuming an exponential falloff of the electronic coupling (Eq. (4)). The open points (Azurin/Ru and CytC/Ru) are taken from Figure 2 and vertically shifted to align with electrochemical data. Note a very good agreement in the distance decay between electrochemical and solution measurements for azurin. The experimental results are reproduced with permission from Refs. [24] and [42].

First, it was discovered that the rate constant saturates to a plateau at distances $R < R^* \simeq 12 - 15$ Å. Surprisingly, one finds that the Dutton radius falls close to the crossover distance

$$R_D \simeq R^*. \tag{7}$$

Second, the reorganization energies measured by electrochemistry are consistently below the "universal" value of 0.8 eV falling in the range $0.2 - 0.5$ eV. The first observation is consistent with the prediction of the dynamical control of electron transfer [43–47] derived for electron-transfer reactions in solution. This general formulation yields the rate constant of electron transfer k_{ET} as the ratio of the nonadiabatic, golden rule rate constant k_{NA} and the correction factor $1 + g$

$$k_{\mathrm{ET}} = (1 + g)^{-1} k_{\mathrm{NA}}. \tag{8}$$

Importantly, the crossover parameter

$$g \propto \tau_X V_e^2 \tag{9}$$

in Eq. (8) is proportional to the product of V_e^2 and the relaxation time τ_X of the dynamic coordinate $X(t)$ supplied experimentally or computationally by the Stokes-shift dynamics [48,49]. Therefore, with decreasing the donor-acceptor distance and thus increasing the electronic coupling V_e, one arrives at the crossover condition $g(R^*) = 1$. At $R < R^*$ the squared electronic coupling V_e^2 cancels out from the nominator and denominator in Eq. (8) and the rate constant switches from the nonadiabatic, distance-dependent function to the limit of Kramers kinetics [50–52]

$$k_{\mathrm{ET}} \propto \tau_X^{-1}. \tag{10}$$

The rate constant reaches a plateau and does not depend on electronic coupling anymore (Figure 4).

Preprints (www.preprints.org) | NOT PEER-REVIEWED | Posted: 14 November 2022 doi:10.20944/preprints202211.0232.v1

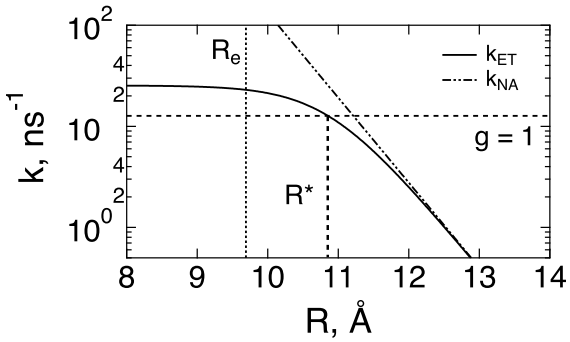

Figure 5. Rate constant of $1 \rightarrow 2$ electron transfer (Eq. (13)) vs the distance between the Cu atom of the active site and the center of mass of tyrosine's phenol ring. The calculated nonadiabatic rate constant $k_{\rm NA}$ (Eq. (5), dash-dotted line) is compared to the full electron-transfer rate constant $k_{\rm ET}$ (Eq. (8), solid line). The horizontal dashed line shows $g(R^*) = 1$, $R^* = 10.9$ Å and the vertical dotted line indicates the equilibrium distance $R_e = \langle R \rangle_1 = 9.7$ Å from MD trajectories.

Even though measurements seem to be qualitatively consistent with the view of the dynamical control of electron transfer, an attempt to fit the data to the standard model [43–47] has produced the Stokes-shift relaxation time $\tau_X \simeq 200$ ns [35], which is much higher than anticipated either from solution measurements [53] or from molecular dynamics simulations of the half redox reaction of cytochrome c [54]. The mystery was resolved by allowing fluctuations of the donor-acceptor distance [41,55]. Such fluctuations produce a new time scale for the problem

$$\tau_\gamma = (\gamma^2 D_R)^{-1}. \tag{11}$$

This is the time required for the redox-active protein to diffuse through the tunneling decay distance γ^{-1} with the translational diffusion constant D_R. The time τ_γ competes with τ_X for the dynamical control of the reaction rate, but, even more importantly, the Stokes-shift relaxation time becomes modified with a factor carrying the information about the protein elasticity in the form of the variance of the donor-acceptor distance $\sigma_R^2 = \langle (\delta R)^2 \rangle$

$$\tau_X \rightarrow \tau_{\rm eff} = \tau_X \exp\left[\tfrac{3}{2}\gamma^2 \langle (\delta R)^2 \rangle\right]. \tag{12}$$

Protein's flexibility enters the theory through both the dynamics of the donor-acceptor distance and its variance. The effective time entering the dynamical crossover parameter g becomes longer for more flexible proteins, thus increasing the crossover distance R^*.

As mentioned above (Eq. (7)), the crossover length, $R^* \simeq 12 - 15$ Å [42], nearly coincides with the maximum distance $\simeq 14 - 15$ Å within which most activated electron-transfer reactions are found in biological energy chains [24,56]. If R^* found by electrochemistry can be extended to intraprotein electron transfer, that would imply that most electron-transfer hops within proteins occur in the limit of dynamical control when tunneling does not affect the rate. Experiments by DeVault and Chance, discussed at the beginning of this section, apply to interprotein electron transfer and might still be controlled by tunneling. However, one faces a number of significant questions, including the issue of the magnitude and temperature dependence of the Stokes-shift relaxation time. Given that the relaxation time becomes slower with lowering temperature, the crossover distance R^* is expected to increase at low temperatures. Therefore, even if interprotein electron transfer is controlled by tunneling at high temperatures, it might fall under the dynamical control with cooling.

The present article extends our previous results [57] for intraprotein electron transfer between tryptophan (Trp) residue of azurin and its active site to a single-residue mutation replacing tryptophan with tyrozine (Tyr). The reaction of transferring the hole from Trp to Cu^I of the active site was studied experimentally by Shih et al [58] and the reaction time of $\tau_{\rm ET} \simeq 31$ ns reported. Trp-Tyr mutation was also attempted, but resulted in no observable

Preprints (www.preprints.org) | NOT PEER-REVIEWED | Posted: 14 November 2022 doi:10.20944/preprints202211.0232.v1

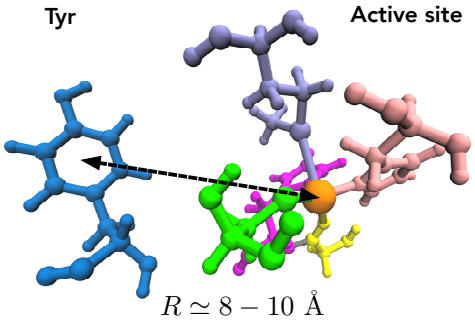

Figure 6. Drawing of the Cu-ligated active site and the tyrosine (Tyr) residue of azurin (PDB 1AZU). The distance between Cu and the center of mass of phenol ring of Tyr is $R_e = 8.6$ Å for the neutral Tyr state and 9.7 Å for the cation radical state Tyr^+.

transition. Here, we study the reaction of electron transfer from the active site of azurin to cation radical Tyr+ replacing Trp in the wild type protein (Figure 6).

The hole on Tyr is experimentally created by photoexcitation of a Re^I-diimine complex labeled as A^* in the following reaction scheme

$$(0)\ A^* - Tyr - Cu^I \rightarrow (1)\ A^- - Tyr^+ - Cu^I \xrightarrow{k_{ET}} A^- - Tyr - Cu^{II}\ (2). \qquad (13)$$

The cation radical Tyr^+ is produced in less than 1 ps, followed with electron transfer from the active site of azurin to Tyr^+. This is the reaction studied here by combining the analytical dynamical theory of electron transfer [59] with classical molecular dynamics (MD) simulations.

2. Dynamical theory of protein electron transfer

The dynamical formulation of the theory of protein electron transfer is complicated by the fact that a number of competing nuclear modes, relaxing on similar time scales, affect the dynamics near the crossing point of the free energy surfaces along the reaction coordinate X. The crossing point specifies the activation barrier and the competing time scales enter the dynamical cross-over parameter g in Eq. (8). The most significant nuclear modes competing in the pre-exponential factor of the rate constant are the medium polarization and the donor-acceptor distance. With the account of these two nuclear modes, the parameter g is given by the following equation [59]

$$g = \frac{2\pi V_e^2 \tau_X}{\hbar \sigma_X} \frac{e^{3\gamma^2 \langle (\delta R)^2 \rangle / 2}}{\sqrt{2\beta \Delta F^\dagger + 4(\tau_X/\tau_R)\gamma^2 \langle (\delta R)^2 \rangle}}, \qquad (14)$$

in which $\sigma_X^2 = 2\lambda k_B T$ is the variance of the electron-transfer energy gap from polarization fluctuations. All parameters in Eq. (14), except for γ, depend on the electron transfer state $i = 1, 2$; this dependence is dropped for brevity. We discuss the magnitude of g for the charge-transfer reaction $1 \rightarrow 2$ shown in Eq. (13). The simulation protocol follows our previous study of wild type azurin and is described in supplementary material (SM). Here, we focus on the results.

The crossover parameter in Eq. (14) depends on the Stokes-shift relaxation time τ_X and the relaxation time of the donor-acceptor dynamics τ_R. Both are calculated as integral relaxation times from the corresponding normalized time correlation functions

$$S_Y^{(i)}(t) = \frac{\langle \delta Y(t) \delta Y(0) \rangle_i}{\langle (\delta Y(0))^2 \rangle_i}, \qquad (15)$$

Table 1. Reorganization energies (eV) for the forward and backward transitions in the charge shift reaction (Eq. (13)) at $T = 300$ K. Also listed are relaxation times (ps), the variances of the donor-acceptor distance (Å^2), and the dynamical crossover parameters (Eq. (14)).

State	λ	λ^{St}	τ_X	τ_R	$\langle R\rangle$	$\langle(\delta R)^2\rangle$	g
$\mathrm{Tyr}^+ - \mathrm{Cu}^{\mathrm{I}}$	1.08	1.33	8.47	18.25	9.69	0.10	11
$\mathrm{Tyr} - \mathrm{Cu}^{\mathrm{II}}$	1.57		10.39	57.98	8.63	0.43	70

where the variable $Y(t)$ is either $X(t)$ or $R(t)$ and $\delta Y(t) = Y(t) - \langle Y\rangle_i$; $\langle\ldots\rangle_i$ specifies an ensemble average in two different electron-transfer states $i = 1,2$ (Eq. (13)). These calculations (see SM) show that electrostatic interactions and the donor-acceptor distance relax on comparable time scales (Table 1).

Another significant parameter is the protein flexibility expressed in terms of the donor-acceptor distance variance $\sigma^2_{R,i} = \langle(\delta R)^2\rangle_i$ (Table 1). The average distance between tyrosine's phenol ring and the Cu atom of the active site $\langle R\rangle_i$ changes somewhat between the two states, but the main difference between two electron-transfer states in terms of distance statistics is in the distance variance. Consistently with our previous simulations of wild type azurine [57], the state with a higher number of water molecules around the residue shows a greater extend of distance flexibility. In the present simulations, a larger number of water molecules was found around neutral Tyr (Figure S10), which is reflected by a broader distribution of donor-acceptor distanced (Figure S3) and a larger distance variance (Table 1).

For the dynamical parameters listed in Table 1 and $\Delta F^\dagger \simeq 0.03$ eV calculated below, we find that the first term under the square root in the denominator of Eq. (14) dominates over the second term. The crossover parameter can be simplified in this case to the following expression in which only the Stokes-shift relaxation time enters the crossover parameter and the rate constant in the dynamics-controlled plateau region (Figure 5)

$$g = \frac{\pi V_e^2}{\hbar\sqrt{\lambda\Delta F^\dagger}}\tau_{\mathrm{eff}}, \tag{16}$$

where τ_{eff} is given by Eq. (12) and g enters the pre-exponential factor of the rate constant according to Eq. (8).

3. Q-model of protein electron transfer

Calculation of the free energy barrier for electron transfer requires constructing the free energy surfaces of electron transfer corresponding to the initial state, $F_1(X)$, and to the final state, $F_2(X)$. The standard approach [27] is to produce crossing Marcus parabolas with the activation barrier in Eq. (6). This approach is, however, not applicable to the energetics of electron transfer in azurin.

The two electron-transfer states in Eq. (13) are characterized by different wetting patterns of the Tyr residue (Figure S11). The consequence of this new physics as that the reorganization energy from the variance of the energy gap becomes state-dependent

$$\lambda_i = \tfrac{1}{2}\beta\langle(\delta X)^2\rangle_i. \tag{17}$$

These two values of the variance reorganization energy are also different from the Stokes-shift reorganization energy [60]

$$2\lambda^{\mathrm{St}} = X_1 - X_2, \tag{18}$$

where $X_i = \langle X\rangle_i$ are two average values of the energy gap calculated from trajectories in equilibrium with the corresponding electron-transfer state $i = 1,2$. In Marcus theory, all three reorganization energies are equal, $\lambda^{\mathrm{St}} = \lambda_1 = \lambda_2$. Their inequality demands an extension to non-parabolic free-energy surfaces accomplished here by the use of the

Preprints (www.preprints.org) | NOT PEER-REVIEWED | Posted: 14 November 2022 doi:10.20944/preprints202211.0232.v1

Q-model of electron transfer [61]. This model stipulates the following inequality between three reorganization energies

$$\lambda_1 < \lambda^{\mathrm{St}} < \lambda_2, \tag{19}$$

where λ_1 and λ_2 can be swapped to match a given reaction. The main requirement for the model to be mapped on a specific physical situation is that the Stokes-shift reorganization energy falls between two variance reorganization energies.

The Q-model is based on three parameters: any two reorganization energies out of λ_i, λ^{St} can be used along with the experimental reaction free energy ΔF_0 to construct $F_i(X)$ (see SM). The reaction free energy ΔF_0 requires the reduction potentials of azurin, equal to $E^0 = 0.341$ V [62], and of $\mathrm{Trp}^+/\mathrm{Trp}^{\cdot}$. The radical cation radical tyrosine is unstable and loses phenolic proton in solution to become the neutral tyrosyl radical $\mathrm{Tyr}^{\cdot}$. The formal potential of $\mathrm{Tyr}^{\cdot}$ is 1.0 V against NHE. The potential for the cation radical has been estimated as 1.38 V in water and even higher, $\simeq 1.8 - 1.9$ V, in a dehydrated, low-dielectric protein environment [63]. The reaction energy thus changes between $\Delta F_0 = -1.04$ eV in the former case and $\Delta F_0 = -1.46$ eV in the latter.

Combining these parameters, one arrives at the non-parabolic free energy surfaces shown in Figure 7. The lower portion of each surface, shown by points, is calculated directly from sampling the energy gap (Eq. (3)) on MD simulation trajectories. In contrast, the upper portions are obtained from the linear relations to which $F_i(X)$ satisfy [21,64,65]

$$F_2(X) = F_1(X) + X. \tag{20}$$

The solid lines in the figure are produced with the Q-model (see SM) which provides a good description of the simulation data. The main result of these calculations is that the forward reaction in the scheme shown in Eq. (13) is essentially activationless, with the activation barrier of $\Delta F^{\dagger} \simeq 7$ meV. Tis result is not modified much if the reduction potential of 1.8 V is adopted for $\mathrm{Trp}^+/\mathrm{Trp}^{\cdot}$ reduction in a dehydrated protein medium. The reaction shifts to the inverted region in this case, resulting in $\Delta F^{\dagger} \simeq 13$ meV (Figure S9). The wetting state of the Tyr pocket inside the protein weakly affects the rate of electron transfer.

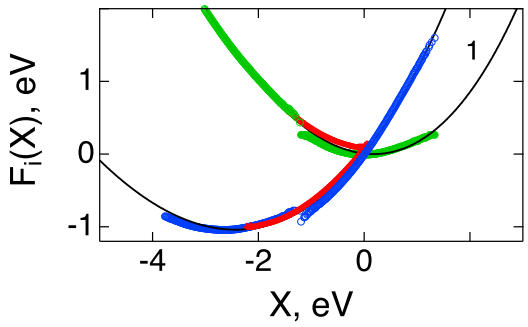

Figure 7. Free energy surfaces of electron transfer calculated in the Q-model (solid lines, see SM) and compared to MD simulations (points). The lower points are from simulations of 1 and 2 states in the reaction scheme in Eq. (13). The upper portions of the simulation data (open points) are obtained from the results around the minima by applying the linear relation from Eq. (20). Red points are from simulations in the intermediate state with $z = 1/2$ in Eq. (21). The calculations are based on the estimated value of the reaction free energy $\Delta F_0 = -1.04$ eV.

We have additionally applied the umbrella sampling technique [65–67] and simulated the system in the state half way between the initial an final states and characterized by the Hamiltonian $H_z = H_1 + z(H_2 - H_1)$ (see SM). The corresponding free energy surface is

$$F_z(X) = F_1(X) + zX \tag{21}$$

Preprints (www.preprints.org) | NOT PEER-REVIEWED | Posted: 14 November 2022 doi:10.20944/preprints202211.0232.v1

which becomes $F_1(X)$ at $z = 0$ and $F_2(X)$ at $z = 1$. The simulation was done at $z = 1/2$. The red points in Figure 7 show $F_1(X) = F_{1/2}(X) - X/2$ and $F_2(X) = F_{1/2}(X) + X/2$.

The rate constant of electron transfer was calculated from Eq. (8) accounting for the nonadiabatic rate constant $k_{\rm NA}$ and the dynamical crossover parameter making the reaction rate independent of the distance in the dynamically controlled regime. The nonadiabatic rate constant was calculated as elsewhere [57] by using the electronic coupling V_e (Eq. (5)) provided by Voityuk [68] (see SM). This calculation yields the reaction time $\tau_{\rm ET} = k_{\rm ET}^{-1} \simeq 40$ ps. This reaction time is similar to $\simeq 40$ ps reported for electron-transfer activationless quenching of photoexcited Trp by heme of myoglobin ($R \simeq 12$ Å) [69], but is much shorter than $\tau_{\rm ET} \simeq 31$ ns reported [58] for the reaction involving Trp residue in wild type azurin. The reaction studied here refers to the equilibrated Tyr^+ and Tyr residues in the corresponding oxidation states. Their wetting to the equilibrium configuration is accomplished on the time scale of $\simeq 150$ ns (Figure S10). This equilibration most likely does not occur in real system since Tyr^+ loses its phenolic proton to become a neutral tyrosyl radical $Tyr^{\cdot}$ [70]. Given how fast electron transfer is, proton-coupled electron transfer [71] does not seem to be required to speed charge transport up. The release of proton might instead follow the electron-induced proton transfer mechanism [72].

If Tyr^+ is deprotonated, the charge-transfer reaction must proceed in an alternative mechanism of creation of the negative anion radical Tyr^- and might be much slower. Indeed, the reduction potential of Tyr/Tyr^- is 0.68 V and the reaction free energy for electron transfer becomes $\Delta F_0 = -0.34$ eV. Assuming the same reorganization parameters as listed in Table 1, this driving force yields the activation barrier of $\Delta F^\dagger = 0.17$ eV and the reaction time of 8 ns. In fact, no reaction was observed for azurin with Tyr mutation [58].

Oxidized tyrosine cation radicals (Tyr^+) are viewed as elements of chains of aromatic residues serving as relay elements to transport oxidizing electron holes to avoid oxidative damage to enzymes' active sites [15,24,58,71,73,74]. Our calculations indicate that electron transfer to oxidized Tyr^+ can be fast, and it should compete with deptotonation of oxidized tyrosine to avoid kinetic bottlenecks. Avoiding wetting of tyrosine sites might be a critical component for the design of such charge transport chains of aromatic residues, as well as the mechanism for regulating the aromatic residue relays [73]. Protein environment can switch charge transport relays on and off by regulating the extent of wetting of tyrosine sites. Given that wetting and drying are slow processes, which take $\sim 150 - 200$ ns in our simulations, falling into an "incorrect" wetting state makes the enzyme inactive over the corresponding waiting time. This phenomenology is known as the dynamic heterogeneity of enzymes established by single-molecule measurements [75–78]. The dynamical heterogeneity is typically linked to the dispersion in catalytic rates due to conformational transitions of time scales exceeding the reaction time. It appears that wetting transitions follow a similar phenomenology since transitions between different wetting states of the active site are much slower than electron-transfer reactions in the corresponding states.

The main result of our simulations and calculations is that electron transfer between Tyr^+ and the active site of azurin is in dynamically controlled regime, that is at the plateau in the distance dependence of the rate constant in Figure 5. The crossover parameters g listed in Table 1 significantly exceed the value $g(R^*) = 1$ for the transition from the dynamics-controlled to the tunneling-controlled regime. The rate constant in the plateau region is significantly lower, at least by an order of magnitude, compared to the result anticipated based on standard nonadiabatic theories of protein electron transfer (Eq. (5)). Electronic tunneling does not affect the rate in this limit and the rate constant is instead affected by the protein identity (dynamics and flexibility).

4. Discussion

Returning to DeVault and Chance experiments, theoretical interpretation of their data by Hopfield [79] and Jortner [80] showed that the change in the Arrhenius slope at low temperatures comes from the quantum nature of nuclear modes coupled to electron transfer. The corresponding independence of the reaction rate of temperature (lower-temperature

Preprints (www.preprints.org) | NOT PEER-REVIEWED | Posted: 14 November 2022 doi:10.20944/preprints202211.0232.v1

part in Figure 1) reflects nuclear tunneling of collective normal-mode vibrations (in contrast to localized, single particle atomic tunneling [81]). The picture following from this analysis, and the shape of rate's temperature dependence, are quite consistent with kinetic data reported by Frauenfelder an co-workers for the rate of CO migration in hemoglobin [82] and cytochrome *c* [83]. In both cases, one observes a low-temperature plateau of the rate attributed to nuclear tunneling (Figure 8). Therefore, it is not electron tunneling that is responsible for the change of the temperature slope in the Arrhenius plot. Electron tunneling occurs at all temperatures and it is only the statistics of nuclear fluctuations that change with temperature allowing nuclear tunneling to occur at low temperatures.

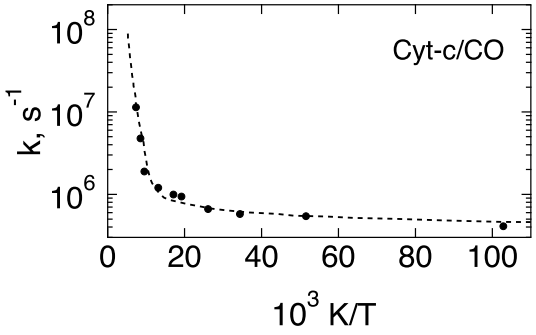

Figure 8. Rate constant for the binding of CO to cytochrome *c* as a function of temperature. Experimental data (points) are taken from Ref. [83], the dashed line is a fit through the data points.

Is it only the statistics of fluctuations that matters? Quoting from Szent-Gyorgyi, "The fuel of life is the electron, or, more exactly, the energy it takes over from photons in photosynthesis; this energy the electron gives up gradually when flowing through the cellular machinery" [84]. To do so, electron must tunnel between localized states in the absence of conduction bands in disordered molecular systems. Tunneling occurs at all temperatures relevant to biology, but the overall transition probability is also affected by the dynamics of barrier crossing, as was established already in the Landau-Zener model of nonadiabatic transitions [19,51]. The dynamics of transversing the region where Born-Oppenheimer electronic terms cross must thus enter the description at some point.

Dynamics of the medium near the tunneling configuration compete with the tunneling time $\simeq \hbar/V_e$ (not to be confused with the time spent by the particle to tunnel through the barrier [85]). The overall observable rate reflects the slowest, rate-determining step in a complex kinetic scheme. It is expressed mathematically in terms of the dynamical crossover parameter g in the pre-exponential factor of the rate constant (Eq. (8)). Even though the rate of tunneling accelerates at shorter donor-acceptor distances, a slower processes of friction-driven barrier crossing dominates in the rate. It is not that tunneling does not exist anymore, but it is not reflected in the reaction rate constant which enters the plateau region at shorter donor-acceptor separations. This is the domain of Kramers' kinetics [50–52] when the relaxation time determines the rate constant pre-exponential factor. The range of donor-acceptor separations $R < R^*$ is where protein dynamics and flexibility affect the rate.

The observation that rates of protein electron hopes are not given by universal parameters applicable to all proteins [25,26] and are, instead, affected by protein identities resonates with a general idea, advocated recently [29], that dynamical aspects can affect rates of enzymatic reactions [30–32]. The existing electron-transfer theories do not allow such dynamical effects for either biological proton or electron transfer since protein dynamics do not enter standard formulations. The picture of dynamical effect on electron transfer allows a departure from this tradition at least in the limited range of distances. The range $R < R^*$ is affected by protein flexibility (Eq. (12)): flexible media must show more propensity for electron transport affected by dynamics. Importantly, this observa-

 doi:10.20944/preprints202211.0232.v1

tion suggests a new design principle for biological energy chains: no reaction speedup can be achieved by placing redox cofactors at distances closer than the crossover distance R^*. This new principle demands a new understanding of conductivity through stacked residues and cofactors in biomolecules. For instance, conducting bacterial nanowires [86] are made of stacked pairs of cytochrome *c* proteins [16,87] with the edge-to-edge distances of 3.4–4.1 within one pair and 5.4–6.1 Å between the pairs. These hopping distances fall within the range $R < R^*$ and raise the issue of medium dynamics affecting conductivity.

In his groundbreaking paper [3] outlining the chemiosmotic theory of oxidative phosphorylation, Mitchell noted that "it represents the result of carrying to its logical conclusion the present trend towards recognizing the equivalent status of supramolecular and molecular features in channeling of chemical processes in living organisms". Theories of electron transfer developed in recent decades have placed their main focus on the "molecular" aspects of the problem, when the supramolecular character of the protein-water and protein-membrane-water media does not show up. Protein itself, in this view, only helps to hold the cofactors in sufficiently rigid active sites, but otherwise produces little effect on electron-transfer kinetics. The present focus brings the "supramolecular" component of the problem back to light. Proteins allow catalytic lowering of the activation barrier [88,89], but also affect the rate constant's pre-exponential factor through protein dynamics (τ_X and τ_R) and protein flexibility ($\langle\langle(\delta R)^2\rangle\rangle$).

5. Conclusions

Electron can tunnel between cofactors of biological energy chains to up to $\simeq$ 21 Å on the millisecond time scale of enzymatic turnover. This tunneling range mostly determines the design principles of biological charge-transfer chains made of redox-active molecules to facilitate cross-membrane transport of electrons. Tunneling distance and redox potentials (reaction Gibbs energy) of the cofactors are viewed as main physical parameters of this design [25,26]. The protein identity, flexibility, or dynamics are missing from this picture assigning universal charge-transport properties to all proteins. Dynamic models of electron transfer challenge this paradigm. Computer simulations of protein electron transfer show that the hopping rate must stay constant within the crossover distance $R < R^* \simeq 11 - 12$ Å. The standard exponential falloff of the rate is restored at $R > R^*$. Energy chains for electron transport are best designed by placing the redox cofactors near the crossover distance R^*. Protein flexibility and dynamics affect the magnitude of the maximum hopping rate within the crossover radius.

Author Contributions: Conceptualization, S.S. and D.M.; methodology, D.M.; software, S.S.; writing, S.S. and D.M.; project administration, D.M.; funding acquisition, D.M. All authors have read and agreed to the published version of the manuscript.

Funding: This research was supported by the National Science Foundation (CHE-2154465). The supercomputer time was provided through Extreme Science and Engineering Discovery Environment (XSEDE) allocation MCB080071 and through ASU's Research Computing.

Data Availability Statement: The data presented in this study are available on request from the corresponding author.

Conflicts of Interest: The authors declare no conflict of interest.The funders had no role in the design of the study; in the collection, analyses, or interpretation of data; in the writing of the manuscript; or in the decision to publish the results.

References

1. de Vault, D.; Chance, B. Studies of phosynthesis using a pulsed laser. I. Temperature dependence of cytochrome oxidation rate in Chromatium. Evidence for tunneling. *Biophys. J.* **1966**, *6*, 825.
2. DeVault, D. *Quantum-mechanical tunneling in biologycal systems*; Cambridge University Press: Cambridge, UK, 1984.
3. Mitchell, P. Coupling of Phosphorylation to Electron and Hydrogen Transfer by a Chemi-Osmotic type of Mechanism. *Nature* **1961**, *191*, 144–148. https://doi.org/10.1038/191144a0.
4. Nicholls, D.G.; Ferguson, S.J. *Bioenergetics4*; Academic Press: Amsterdam, 2013.
5. Szent-Gyorgyi, A. The study of energy levels in biochemistry. *Nature* **1941**, *148*, 157–159. https://doi.org/10.1038/148157a0.

6. Pethig, R.; Szent-Györgyi, A. Electronic properties of the casein-methylglyoxal complex. *Proceedings of the National Academy of Sciences* **1977**, *74*, 226–228. https://doi.org/10.1073/pnas.74.1.226.
7. McGinness, J.; Corry, P.; Proctor, P. Amorphous Semiconductor Switching in Melanins. *Science* **1974**, *183*, 853–855. https://doi.org/10.1126/science.183.4127.853.
8. Barbara, P.F.; Olson, E.J.C. Experimental electron transfer kinetics in a DNA environment. *Adv. Chem. Phys.* **2016**, *107*, 647–676. https://doi.org/10.1002/9780470141663.ch13.
9. Bostick, C.D.; Mukhopadhyay, S.; Pecht, I.; Sheves, M.; Cahen, D.; Lederman, D. Protein bioelectronics: a review of what we do and do not know. *Rep. Prog. Phys.* **2018**, *81*, 026601.
10. Moser, C.C.; Keske, J.M.; Warncke, K.; Farid, R.S.; Dutton, P.L. Nature of biological electron transfer. *Nature* **1992**, *355*, 796–802.
11. Gray, H.B.; Winkler, J.R. Long-range electron transfer. *Proc. Natl. Acad. Sci.* **2005**, *102*, 3534–3539.
12. Lovley, D.R.; Walker, D.J.F. Geobacter Protein Nanowires. *Frontiers in Microbiology* **2019**, *10*, 2078. https://doi.org/10.3389/fmicb.2019.02078.
13. Wang, F.; Gu, Y.; O'Brien, J.P.; Yi, S.M.; Yalcin, S.E.; Srikanth, V.; Shen, C.; Vu, D.; Ing, N.L.; Hochbaum, A.I.; et al. Structure of Microbial Nanowires Reveals Stacked Hemes that Transport Electrons over Micrometers. *Cell* **2019-04**, *177*, 361–369.e10. https://doi.org/10.1016/j.cell.2019.03.029.
14. Giese, B.; Graber, M.; Cordes, M. Electron transfer in peptides and proteins. *Curr. Opin. Chem. Biol.* **2008**, *12*, 755–759.
15. Shipps, C.; Kelly, H.R.; Dahl, P.J.; Yi, S.M.; Vu, D.; Boyer, D.; Glynn, C.; Sawaya, M.R.; Eisenberg, D.; Batista, V.S.; et al. Intrinsic electronic conductivity of individual atomically resolved amyloid crystals reveals micrometer-long hole hopping via tyrosines. *Proc. Natl. Acad. Sci. USA* **2021**, *118*, e2014139118. https://doi.org/10.1073/pnas.2014139118.
16. Dahl, P.J.; Yi, S.M.; Gu, Y.; Acharya, A.; Shipps, C.; Neu, J.; O'Brien, J.P.; Morzan, U.N.; Chaudhuri, S.; Guberman-Pfeffer, M.J.; et al. A 300-fold conductivity increase in microbial cytochrome nanowires due to temperature-induced restructuring of hydrogen bonding networks. *Sci. Adv.* **2022**, *8*, eabm7193. https://doi.org/10.1126/sciadv.abm7193.
17. Gamow, G. Zur Quantentheorie des Atomkernes. *Z. Phys.* **1928**, *51*, 204–212. https://doi.org/10.1007/bf01343196.
18. Lax, M. The Frank-Condon principle and its application to crystals. *J. Chem. Phys.* **1952**, *20*, 1752–1760.
19. Landau, L.D.; Lifshits, E.M. *Quantum Mechanics: Non-Relativistic Theory*; Pergamon Press: Oxford, 1977.
20. Hoff, A.J.; Deisenhofer, J. Photophysics of photosynthesis. *Phys. Rep.* **1997**, *287*, 1–247.
21. Warshel, A. Dynamics of reactions in polar solvents. Semiclassical trajectory studies of electron-transfer and proton-transfer reactions. *J. Phys. Chem.* **1982**, *86*, 2218–2224.
22. Skourtis, S.S.; Waldeck, D.H.; Beratan, D.N. Fluctuations in biological and bioinspired electron-transfer reactions. *Annu. Rev. Phys. Chem.* **2010**, *61*, 461–485. https://doi.org/10.1146/annurev.physchem.012809.103436.
23. Winkler, J.R.; Gray, H.B. Electron flow through metalloproteins. *Chem. Rev.* **2014**, *114*, 3369–3380.
24. Gray, H.B.; Winkler, J.R. Functional and protective hole hopping in metalloenzymes. *Chem. Sci.* **2021**, *12*, 13988–14003. https://doi.org/10.1039/d1sc04286f.
25. Page, C.C.; Moser, C.C.; Chen, X.X.; Dutton, P.L. Natural engineering principles of electron tunneling in biological oxidation-reduction. *Nature* **1999**, *402*, 47–52.
26. Moser, C.C.; Anderson, J.R.; Dutton, P.L. Guidelines for tunneling in enzymes. *Biochim. Biophys. Acta - Bioenergetics* **2010**, *1797*, 1573–1586. https://doi.org/10.1016/j.bbabio.2010.04.441.
27. Marcus, R.A.; Sutin, N. Electron transfer in chemistry and biology. *Biochim. Biophys. Acta* **1985**, *811*, 265–322.
28. Pauling, L. Molecular architecture and biological reactions. *Chem. Eng. News* **1946**, *24*, 1375–1377.
29. Klinman, J.P.; Kohen, A. Hydrogen tunneling links protein dynamics to enzyme catalysis. *Ann. Rev. Biochem.* **2013**, *82*, 471–496.
30. Kern, D.; Zuiderweg, E.R.P. The role of dynamics in allosteric regulation. *Curr. Opin. Struct. Biol.* **2003**, *13*, 748–757.
31. Henzler-Wildman, K.A.; Thai, V.; Lei, M.; Ott, M.; Wolf-Watz, M.; Fenn, T.; Pozharski, E.; Wilson, M.A.; Petsko, G.A.; Karplus, M.; et al. Intrinsic motions along an enzymatic reaction trajectory. *Nature* **2007**, *450*, 838–844.
32. Kohen, A. Role of Dynamics in Enzyme Catalysis: Substantial versus Semantic Controversies. *Acc. Chem. Res.* **2015**, *48*, 466–473.
33. Finklea, H.O. Electrochemistry of organized monolayers of thiols and related molecules on electrodes. *Electroanal. Chem.: A series of advances* **1996**, *19*, 109–335.
34. Murgida, D.H.; Hildebrandt, P. Redox and redox-coupled processes of heme proteins and enzymes at electrochemical interfaces. *Phys. Chem. Chem. Phys.* **2005**, *7*, 3773–3784. https://doi.org/10.1039/b507989fPMID-16358026.
35. Waldeck, D.H.; Khoshtariya, D.E. Fundamental Studies of Long- and Short-Range Electron Exchange Mechanisms between Electrodes and Proteins. In *Applications of Electrochemistry and Nanotechnology in Biology and Medicine I*; Springer New York: New York, NY, 2011; pp. 105–238.
36. Alvarez-Paggi, D.; Hannibal, L.; Castro, M.A.; Oviedo-Rouco, S.; Demicheli, V.; Tórtora, V.; Tomasina, F.; Radi, R.; Murgida, D.H. Multifunctional cytochrome c: Learning new tricks from an old dog. *Chem. Rev.* **2017**, *117*, 13382–13460. https://doi.org/10.1021/acs.chemrev.7b00257.
37. Buhrke, D.; Hildebrandt, P. Probing structure and reaction dynamics of proteins using time-resolved resonance raman spectroscopy. *Chem. Rev.* **2019**, *120*, 3577–3630. https://doi.org/10.1021/acs.chemrev.9b00429.
38. Murgida, D.H.; Hildebrandt, P. Proton-coupled electron transfer of cytochrome c. *J. Am. Chem. Soc.* **2001**, *123*, 4062–4068. https://doi.org/10.1021/ja004165j.

39. Chi, Q.; Zhang, J.; Andersen, J.E.T.; Ulstrup, J. Ordered assembly and controlled electron transfer of the blue copper protein azurin at gold (111) single-crystal substrates. *J. Phys. Chem. B* **2001**, *105*, 4669–4679.
40. Wei, J.J.; Liu, H.; Niki, K.; Margoliash, E.; Waldeck, D.H. Probing electron tunneling pathways: Electrochemical study of rat heart cytochrome *c* and its mutant on pyridine-terminated SAMs. *J. Phys. Chem. B* **2004**, *108*, 16912–16917.
41. Zitare, U.A.; Szuster, J.; Santalla, M.C.; Morgada, M.N.; Vila, A.J.; Murgida, D.H. Dynamical effects in metalloprotein heterogeneous electron transfer. *Electrochim. Acta* **2020**, *342*, 136095.
42. Alvarez-Paggi, D.; Zitare, U.; Murgida, D.H. The role of protein dynamics and thermal fluctuations in regulating cytochrome c/cytochrome c oxidase electron transfer. *Biochim. Biophys. Acta - Bioenergetics* **2014**, *1837*, 1196–1207.
43. Zusman, L.D. Outer-sphere electron transfer in polar solvents. *Chem. Phys.* **1980**, *49*, 295–304.
44. Sumi, H.; Marcus, R.A. Dynamical effects in electron transfer reactions. *J. Chem. Phys* **1986**, *84*, 4894–4914.
45. Hynes, J.T. Outer-sphere electron-transfer reactions and frequency-dependent friction. *J. Phys. Chem.* **1986**, *90*, 3701–3706.
46. Rips, I.; Jortner, J. Dynamic solvent effects on outer-sphere electron transfer. *J. Chem. Phys.* **1987**, *87*, 2090–2104.
47. Yan, Y.J.; Sparpaglione, M.; Mukamel, S. Solvation dynamics in electron-transfer, isomerization, and nonlinear optical processes: a unified Liouville-space theory. *J. Phys. Chem.* **1988**, *92*, 4842–4853. https://doi.org/10.1021/j100328a010.
48. van der Zwan, G.; Hynes, J.T. Time-dependent fluorescence solvent shifts, dielectric friction, and nonequilibrium solvation in polar solvents. *J. Phys. Chem.* **1985**, *89*, 4181–4188.
49. Maroncelli, M. The dynamics of solvation in polar liquids. *J. Mol. Liq.* **1993**, *57*, 1–37.
50. Kramers, H. Brownian motion in a field of force and the diffusion model of chemical reactions. *Physica* **1940**, *7*, 284–304.
51. Frauenfelder, H.; Wolynes, P.G. Rate theories and puzzles of hemeprotein kinetics. *Science* **1985**, *229*, 337–345.
52. Hänggi, P.; Talkner, P.; Borkovec, M. Reaction-rate theory: fifty years after Kramers. *Rev. Mod. Phys.* **1990**, *62*, 251–341. https://doi.org/10.1103/revmodphys.62.251.
53. Jimenez, R.; Fleming, G.R.; Kumar, P.V.; Maroncelli, M. Femtosecond solvation dynamics of water. *Nature* **1994**, *369*, 471–473.
54. Seyedi, S.; Waskasi, M.M.; Matyushov, D.V. Theory and electrochemistry of cytochrome *c*. *J. Phys. Chem. B* **2017**, *121*, 4958–4967. https://doi.org/10.1021/acs.jpcb.7b00917.
55. Matyushov, D.V. Dynamical effects in protein electrochemistry. *J. Phys. Chem. B* **2019**, *123*, 7290–7301. https://doi.org/10.1021/acs.jpcb.9b04516.
56. Page, C.C.; Moser, C.C.; Dutton, P.L. Mechanism for electron transfer within and between proteins. *Curr. Opinion in Biology* **2003**, *7*, 551.
57. Sarhangi, S.M.; Matyushov, D.V. Theory of protein charge transfer: Electron transfer between tryptophan residue and active site of azurin. *J. Phys. Chem. B* **2022**, p. submitted. https://doi.org/10.26434/chemrxiv-2022-fnfck.
58. Shih, C.; Museth, A.K.; Abrahamsson, M.; Blanco-Rodriguez, A.M.; Bilio, A.J.D.; Sudhamsu, J.; Crane, B.R.; Ronayne, K.L.; Towrie, M.; Vlček, A.; et al. Tryptophan-accelerated electron flow through proteins. *Science* **2008**, *320*, 1760–1762. https://doi.org/10.1126/science.1158241.
59. Matyushov, D.V. Conformational dynamics modulating electron transfer. *J. Chem. Phys.* **2022**, *157*, 095102. https://doi.org/10.1063/5.0102707.
60. LeBard, D.N.; Matyushov, D.V. Protein-water electrostatics and principles of bioenergetics. *Phys. Chem. Chem. Phys.* **2010**, *12*, 15335–15348.
61. Matyushov, D.V.; Voth, G.A. Modeling the free energy surfaces of electron transfer in condensed phases. *J. Chem. Phys.* **2000**, *113*, 5413. https://doi.org/10.1063/1.1289886.
62. Garner, D.K.; Vaughan, M.D.; Hwang, H.J.; Savelieff, M.G.; Berry, S.M.; Honek, J.F.; Lu, Y. Reduction potential tuning of the blue copper center in Pseudomonas Aeruginosa azurin by the axial methionine as probed by unnatural amino acids. *J. Am. Chem. Soc.* **2006**, *128*, 15608–15617. https://doi.org/10.1021/ja062732i.
63. Tommos, C.; Babcock, G.T. Proton and hydrogen currents in photosynthetic water oxidation. *Biochim. Biophys. Acta - Bioenergetics* **2000**, *1458*, 199–219. https://doi.org/10.1016/s0005-2728(00)00069-4PMID-10812034.
64. Tachiya, M. Relation between the electron-transfer rate and the free energy change of reaction. *J. Phys. Chem.* **1989**, *93*, 7050–7052.
65. Small, D.W.; Matyushov, D.V.; Voth, G.A. The theory of electron transfer: What may be missing? *J. Am. Chem. Soc.* **2003**, *125*, 7470–7478. https://doi.org/10.1021/ja029595j.
66. Allen, M.P.; Tildesley, D.J. *Computer Simulation of Liquids*; Clarendon Press: Oxford, 1996.
67. Kuharski, R.A.; Bader, J.S.; Chandler, D.; Sprik, M.; Klein, M.L.; Impey, R.W. Molecular model for aqueous ferrous-ferric electron transfer. *J. Chem. Phys.* **1988**, *89*, 3248–3257.
68. Voityuk, A.A. Electron transfer between [4Fe–4S] clusters. *Chem. Phys. Lett.* **2010**, *495*, 131–134. https://doi.org/10.1016/j.cplett.2010.06.057.
69. Consani, C.; Auböck, G.; Mourik, F.v.; Chergui, M. Ultrafast tryptophan-to-heme electron transfer in myoglobins revealed by UV 2D spectroscopy. *Science* **2013**, *339*, 1586–1589. https://doi.org/10.1126/science.1230758.
70. Hoganson, C.W.; Tommos, C. The function and characteristics of tyrosyl radical cofactors. *Biochim. Biophys. Acta - Bioenergetics* **2004**, *1655*, 116–122. https://doi.org/10.1016/j.bbabio.2003.10.017.
71. Stubbe, J.; Nocera, D.G.; Yee, C.S.; Chang, M.C.Y. Radical Initiation in the Class I Ribonucleotide Reductase: Long-Range Proton-Coupled Electron Transfer? *Chem. Rev.* **2003**, *103*, 2167–2202. https://doi.org/10.1021/cr020421u.
72. Matyushov, D.V.; Newton, M.D. Electron-induced proton transfer. *J. Phys. Chem. B* **2021**, *125*, 12264–12273.

73. Bollinger, M.J. Electron relay in proteins. *Science* **2008**, *320*, 1730–1731. https://doi.org/10.1126/science.1160001.
74. Zhang, B.; Ryan, E.; Wang, X.; Song, W.; Lindsay, S. Electronic transport in molecular wires of precisely controlled length built from modular proteins. *ACS Nano* **2022**, *16*, 1671–1680. https://doi.org/10.1021/acsnano.1c10830.
75. Min, W.; English, B.P.; Luo, G.; Cherayil, B.J.; Kou, S.C.; Xie, X.S. Fluctuating enzymes: Lessons from single-molecule studies. *Acc. Chem. Res.* **2005**, *38*, 923–931.
76. Engelkamp, H.; Hatzakis, N.S.; Hofkens, J.; De Schryver, F.C.; Nolte, R.J.M.; Rowan, A.E. Do enzymes sleep and work? *Chem. Commun.* **2006**, *327*, 935–6.
77. Flomenbom, O.; Velonia, K.; Loos, D.; Masuo, S.; Cotlet, M.; Engelborghs, Y.; Hofkens, J.; Rowan, A.E.; Nolte, R.J.M.; Van der Auweraer, M.; et al. Stretched exponential decay and correlations in the catalytic activity of fluctuating single lipase molecules. *Proceedings of the National Academy of Sciences of the United States of America* **2005**, *102*, 2368–2372.
78. Grossman-Haham, I.; Rosenblum, G.; Namani, T.; Hofmann, H. Slow domain reconfiguration causes power-law kinetics in a two-state enzyme. *Proc. Natl. Acad. Sci. USA* **2018**, *115*, 513–518. https://doi.org/10.1073/pnas.1714401115PMID-29298911.
79. Hopfield, J.J. Electron transfer between biological molecules by thermally activated tunneling. *Proc. Nat. Acad. Sci.* **1974**, *71*, 3640.
80. Jortner, J. Temperature dependent activation energy for electron transfer between biological molecules. *J. Chem. Phys.* **1976**, *64*, 4860–4867.
81. Jortner, J.; Ulstrup, J. Dynamics of nonadiabatic atom transfer in biological systems. Carbon monoxide binding to hemoglobin. *J. Am. Chem. Soc.* **1979**, *101*, 3744–3754. https://doi.org/10.1021/ja00508a007.
82. Alberding, N.; Austin, R.H.; Beeson, K.W.; Chan, S.S.; Eisenstein, L.; Frauenfelder, H.; Nordlund, T.M. Tunneling in ligand binding to heme proteins. *Science* **1976**, *192*, 1002–1004. https://doi.org/10.1126/science.1273579.
83. Frauenfelder, H. Molecular tunneling in heme proteins. In *Tunneling in Biological Systems*; Chance, B.; DeVault, D.; Frauenfelder, H.; Marcus, R.A.; J.R.Schrieffer.; N.Sutin., Eds.; Academic Press: New York, 1979; pp. 627–649. https://doi.org/10.1016/b978-0-12-167860-9.50051-3.
84. Szent-Györgyi, A. *Bioelectronics. A Study in Cellular Regulations, Defense, and Cancer*; Academic Press: New York, NY, 1968.
85. Landauer, R.; Martin, T. Barrier interaction time in tunneling. *Rev. Mod. Phys.* **1994**, *66*, 217–228. https://doi.org/10.1103/RevModPhys.66.217.
86. Lovley, D.R. Electrically conductive pili: Biological function and potential applications in electronics. *Curr. Opin. Electrochem.* **2017**, *4*, 190–198. https://doi.org/10.1016/j.coelec.2017.08.015.
87. Yalcin, S.E.; Malvankar, N.S. The blind men and the filament: Understanding structures and functions of microbial nanowires. *Cur. Opin. Chem. Biol.* **2020**, *59*, 193–201. https://doi.org/10.1016/j.cbpa.2020.08.004.
88. Gray, H.B.; Winkler, J.R. Electron tunneling through proteins. *Quart. Rev. Biophys.* **2003**, *36*, 341–372.
89. Matyushov, D.V. Protein electron transfer: is biology (thermo)dynamic? *J. Phys.: Condens. Matter* **2015**, *27*, 473001. https://doi.org/10.1088/0953-8984/27/47/473001.